Thermoelasticity in organic semiconductors determined with terahertz spectroscopy and quantum quasi-harmonic simulations

Thermoelasticity in Organic Semiconductors Determined with Terahertz Spectroscopy and Quantum Quasi-Harmonic Simulations

Peter A. Banks,[†] Jefferson Maul,[‡] Mark T. Mancini,[†] Adam C. Whalley,[†]

Alessandro Erba,[‡] and Michael T. Ruggiero[*,†]

[†]*Department of Chemistry, University of Vermont, 82 University Place, Burlington, Vermont 05405, United States of America*

[‡]*Dipartimento di Chimica, Universitá di Torino, via Giuria 5, 10125 Torino, Italy*

E-mail: Michael.Ruggiero@uvm.edu

Phone: +1 (802) 656-0276

Abstract

The thermomechanical response of organic semiconducting solids is an essential aspect to consider in the design of materials for advanced applications, and in particular, flexible electronics. The non-covalent intermolecular forces that exist in organic solids not only result in a diverse set of mechanical properties, but also a critical dependence of those same properties on temperature. However, studying the thermoelastic response of solids is experimentally challenging, often requiring large single-crystals and sensitive experimental apparatus. An alternative contactless approach involves using low-frequency vibrational spectroscopy to characterize the underlying intermolecular forces, and then combining this information with solid-state density functional theory simulations to retrieve the mechanical response of materials. This methodology leverages recent advances in the quasi-harmonic approximation to predict the temperature evolution of crystalline structures, dynamics, and associated forces, and then utilizes this information to determine the elastic tensor as a function of temperature. Here, this methodology is illustrated for two prototypical organic semiconducting crystals, rubrene and BTBT, and suggests a new alternative means to characterizing the thermoelastic response of organic materials.

Introduction

Organic semiconductors (OSCs) are increasingly finding use in a large number of applications, including photovoltaics and advanced display technologies[1,2] – and, more recently, flexible electronics.[3–5] In contrast to traditional inorganic semiconductors, OSCs can be fabricated in high-yields at low-temperatures using low-cost solution processing methods, which enables the use of flexible substrates.[5,6] In addition, the lack of strong intermolecular interactions (e.g., covalent bonds in crystalline silicon) makes OSCs well-suited for use in flexible applications. However, the presence of weak intermolecular forces alone does not necessarily translate into mechanically soft materials, and the reality is that those same forces

result in a broad spectrum of mechanical properties, ranging from hard, brittle solids to soft, fully deformable materials.[7–10] It is therefore critical that a thorough understanding of the fundamental atomic-level forces responsible for the mechanical response of OSCs be well-understood in order to fully realize their potential applications.

In many cases, OSCs exist in the crystalline phase, with the individual molecules bound through weak intermolecular forces. Just like many other molecular crystals, OSCs exhibit a rich set of structural and thermomechanical phenomena that drive many common bulk phase properties, such as polymorphism and solid-state phase transitions.[11–15] The origin of this diversity lies in the weak intermolecular interactions present in these materials. Unlike covalent bonds, which are relatively strong (ca. $200 - 500\,\mathrm{kJ\ mol^{-1}}$), the intermolecular coordinate is dominated by weak interactions (ca. $< 50\,\mathrm{kJ\ mol^{-1}}$) such as hydrogen bonds, London dispersion forces, and related van der Waals forces. This makes the intermolecular coordinate much softer compared to inorganic semiconductors. Additionally, these interactions are often highly anharmonic,[16,17] which results in the strong temperature-dependence of many phenomena near ambient conditions, for example, thermal expansion.[18] Thus, the intermolecular potential is pivotal to not only understanding the mechanical properties of solids, but also how such properties are affected by external conditions, such as temperature.

While it is clearly critical that the mechanical properties of OSCs be studied, characterizing them can be difficult, requiring large single-crystals, delicate sample preparation, and specialized experimental instrumentation.[19–24] These measurements are made significantly more challenging when additional parameters, for example temperature and pressure, must also be considered. An alternative approach, given the direct dependence of mechanical properties on intermolecular forces, would be to characterize the underlying forces themselves, followed by the determination of the mechanical behavior using this information. Terahertz (or far-IR, $0.1 - 10\,\mathrm{THz}$ or $3 - 333\,\mathrm{cm^{-1}}$) vibrational spectroscopy has proven to be a powerful method for the characterization of intermolecular forces in molecular solids.[25,26] An extension of mid-IR spectroscopy to lower frequencies, terahertz spectroscopy probes large-

amplitude complex motions of entire molecules that efficiently explore a large portion of the potential energy hypersurface. Recently, the link between low-frequency motions and the mechanical properties of materials has been increasingly elucidated.[27–30] While this connection is somewhat intuitive, as both are directly dependent on the interatomic forces, it is the large-amplitude phonon modes present at terahertz frequencies that makes this specific vibrational technique particularly well-suited to characterize mechanical effects.

Due to the low-energy nature of terahertz vibrations, these modes are often highly excited at ambient conditions (298 K $\approx$ 6.2 THz). Indeed, it is precisely these excited low-frequency modes that are responsible for thermal expansion phenomena.[31] Because of this, and the underlying anharmonicity in the vibrational modes, experimental terahertz spectra are often strongly influenced by temperature, reflecting the changes in the intermolecular forces.[32–35] While quantum mechanical simulations can effectively predict the structures and terahertz spectra at very low-temperatures, it has traditionally been unable to capture the temperature-dependent effects, such as peak shifting. However, recently the temperature-dependent structures and low-frequency dynamics of organic solids have been predicted with periodic density functional theory (DFT) through the quasi-harmonic approximation (QHA) method.[31,36–38] While DFT simulations are fundamentally performed at 0 K (due to the Born-Oppenheimer approximation), temperature-dependent structures and dynamics can be effectively modeled by capturing intermolecular anharmonicity through a series of constrained volume optimization and frequency analyses.[39,40] Through minimization of the temperature- and volume-dependent Helmholtz free energy, the structural and dynamical evolution of crystals as a function of temperature can be obtained.

Evaluating the QHA results using temperature-dependent single-crystal X-ray crystallography and terahertz time-domain spectroscopy allows for the validation of the predicted forces as a function of temperature. In this study, this validation is then used as the basis for computing the thermoelastic response of OSC solids, specifically crystalline rubrene and BTBT ([1]benzothieno[3,2-b][1]benzothiophene). The results highlight the advantages

of this indirect contactless methodology for providing comparable results to direct mechanical measurements, opening the door for further studies into this exciting class of advanced materials.

Methods

Experimental

Synthesis of BTBT

Preparation of BTBT from o-chlorobenzaldehyde followed the synthesis reported by Saito.[41] Sodium hydrosulfide hydrate (114.0 g, 1.42 mol) and o-chlorobenzaldehyde (100.0 g, 0.710 mol) in 200 mL of *N*-methyl-2-pyrrolidone (NMP) were heated at 80°C for 1 h, followed by 10 h at 180°C. The resulting solution was poured into a saturated aqueous ammonium chloride solution (1.0 L, 7.4 M), and the product extracted with toluene. The extracted yellow solution was washed with water, and subsequently dried over magnesium sulfate. The resulting yellow solid (8.0 g) was recrystallized in toluene to yield colorless platelet crystals suitable for single-crystal X-ray experiments.

Single-Crystal X-ray Diffraction

All diffraction experiments were performed using a Bruker AXS single-crystal diffractometer. Monochromatic Mo K_α radiation ($\lambda = 0.70926$Å) was used and detected using a SMART APEX CCD. The temperature was controlled using a liquid nitrogen cold finger (Oxford Instruments). Absorption corrections were performed using SADABS,[42] and the data were also corrected for Lorentz and polarization effects. The structures were solved using direct methods with SHELXTL,[?] and the structures refined anisotropically. Subsequently, the hydrogens were found based on residual electron density, and the structures refined isotropically.

Terahertz Time-Domain Spectroscopy

Crystalline rubrene was purhcased from Sigma-Aldrich, and used as-received. The solid samples were prepared for experimental spectroscopy measurements by first mixing with polytetrafluoroethylene (PTFE) to an approximate 3% w/w concentration. The samples were then ground using a mortar and pestle to homogenize the sample and to reduce particle size in order to minimize scattering effects. The resulting powdered mixture was pressed using an hydraulic press, yielding 3 mm free-standing pellets with a diameter of 13 mm.

Experimental terahertz time-domain spectroscopy experiments were performed using a commercial Teraflash Pro spectrometer (Toptica Photonics AG). A pair of fiber-coupled photoconductive antennae were implemented in a free-space optical setup, consisting of two-pairs of gold off-axis parabolic mirrors, which serve to collimate and focus the terahertz radiation on the samples and receiver module, respectively. To minimize absorption from atmospheric water vapor, the entire optical path was enclosed and continuously purged with dry nitrogen gas for the duration of the measurements. Cryogenic measurements were performed using a closed-cycle cryostat (Cryocool Industries). For each measurement, 20000 time-domain waveforms were averaged, and subsequently Fourier transformed to yield a frequency-domain terahertz power spectrum. This power spectrum was then divided by a corresponding blank (PTFE) spectrum, yielding an absorption spectrum. This procedure was repeated in quadruplicate, and the presented spectra are a result of the final average of the four frequency-domain absorption spectrum.

Theoretical

All simulations were performed using the fully-periodic CRYSTAL17 software package.[43] The simulations utilized either the GGA PBE[44] and hybrid PBE0[45] density functionals, coupled with the Grimme D3-BJ dispersion correction.[46,47] The 6-31G(d,p) basis set[48,49] was used for crystalline rubrene, while the larger 6-311G(2d,2p) basis set[50] was used for crystalline BTBT. All simulations were started from low-temperature (100 K) experimental single-crystal X-ray

diffraction-determined structures, and initially underwent a full structural relaxation with no constraints outside of space group symmetry, with a convergence criterion of $\Delta E < 10^{-8}$ a.u. Vibrational analyses were performed numerically using a two-point scheme within the harmonic approximation,[51,52] with a convergence criterion of $\Delta E < 10^{-10}$ a.u.

The QHA simulations were initialized from the fully-relaxed structures, and were performed using a fully-automated procedure.[39,40,53,54] Strained structures corresponding to -2%, 0%, $+2\%$, and $+4\%$ volume increments (with respect to the fully-optimized structures), and a constrained volume optimization was performed. Subsequently, the dynamics were evaluated, again using the two-point numerical differentiation, and through the evolution of the vibrational modes the volume-dependent Helmholtz free energy was determined. By minimizing this with respect to temperature, the predicted structural and dynamical evolution as a function of volume is mapped to temperature values, yielding the effect temperature dependence of these properties.

The thermoelastic response was determined by using the temperature-dependent structures predicted from the QHA calculations as a starting point. Elastic moduli (i.e. elements of the fourth-rank elastic tensor) at temperature T were determined by performing a fully-automated elastic analysis[55,56] on top of the corresponding equilibrium structure with volume $V(T)$ by following a so-called quasi-static approach:[57]

$$C_{vu}(T) = \frac{1}{V(T)} \left. \frac{\partial^2 E}{\partial \eta_v \partial \eta_u} \right|_{\boldsymbol{\eta}=\mathbf{0}} \tag{1}$$

where the thermal expansion of the system $V(T)$ still has to be determined from the quasi-harmonic approximation but the energy derivatives with respect to strain components are computed in terms of static internal energy E instead of free energy F. This approximation drastically reduces the computational cost of thermo-elastic calculations but at the same time allows to take into account a significant fraction of thermal effects on the elastic response of the system.

Results and Discussion

Rubrene

Structural Analysis

Rubrene is a polycyclic aromatic molecule containing a fully conjugated tetracene core and four phenyl substituents (**Figure 1**). It is one of the most widely studied OSCs, and has one of the highest carrier mobilities of known OSCs at room temperature, with reported values ranging from $10 - 40\,\mathrm{cm^2\,V^{-1}\,s^{-1}}$.[58] The origins of the favorable electronic properties arise from a combination of both the molecular and bulk structures.

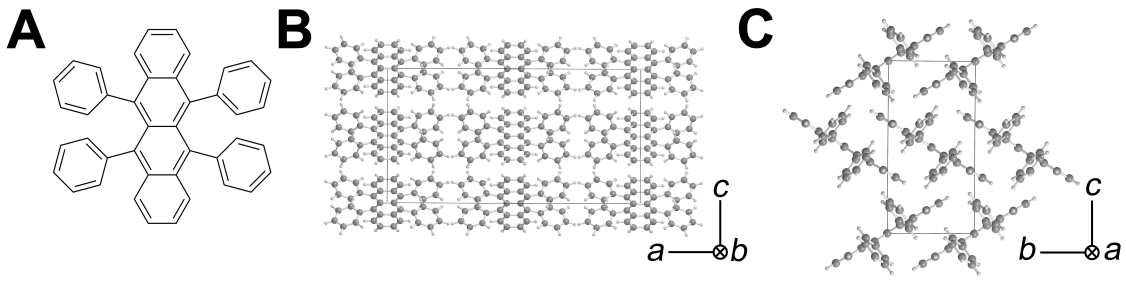

Figure 1: Molecular structure (**A**), unit cell structure (**B**), and alternative view showing herringbone packing (**C**) of rubrene.

Rubrene crystallizes in the orthorhombic *Cmca* space group (**Figure 1**), with 2 molecules in the unit cell, and single-crystal X-ray diffraction-determined lattice parameters of $a = 26.79\,\text{Å}$, $b = 7.17\,\text{Å}$, and $c = 14.21\,\text{Å}$ at $100\,\mathrm{K}$.[59] Rubrene does not contain any permanent dipoles, and as such the crystal structure is dominated entirely by weak non-covalent van der Waals forces, primarily London dispersion and π-stacking interactions.

The molecules pack in a herringbone pattern, with the tetracene cores arranged in alternating layers as shown in **Figure 1**. The tetracene cores are organized in the b and c directions, with an angle between the tetracene cores and the ab plane of 30.76°, in order to maximize π-overlap with adjacent molecules. Additionally, it is also important to consider the substituent phenyl rings, which are oriented nearly perpendicular to the tetracene core. These phenyl groups are arranged in an dovetail manner along the a-direction, where

they form an interlocking ribbon that runs in parallel to the tetracene cores throughout the crystal.

An important first metric for the computational evaluation of chemical systems is a geometry relaxation, which provides a measure of the accuracy of the utilized computational framework as it indicates the location of the minimum in the potential energy hypersurface. In the case of rubrene, the structure was fully-optimized with no constraints outside of space group symmetry using the 6-31G(d,p) basis set and PBE functional, coupled with the D3 dispersion correction. The solid-state DFT optimized structure is in good general agreement with the experimental 100 K structure, with an average error in the unit cell vectors of -1.46%. It is important to note that the optimization resulted in a contraction of all three cell axes, with individual errors in a, b, and c of -1.82%, -0.57%, and -2.01%, respectively. This is somewhat expected, as the DFT simulations are performed at an effective temperature of 0 K and in the absence of zero-point motion, while the experimental structure was obtained at 100 K.

Low-Frequency Dynamics

While the structural optimization provides validation in the correct identification of the potential energy minimum, it only provides indirect holistic information about the interatomic forces. Vibrational spectroscopy is a powerful tool for directly probing interatomic forces, as the vibrational frequencies are directly dependent on the curvature of the vibrational potential energy. Terahertz vibrational spectroscopy is especially powerful in this regard, as the motions that occur at terahertz frequencies are often delocalized to a large extent, enabling the study of weak non-covalent interactions.

The experimental THz-TDS spectrum of rubrene exhibits three well-resolved features at 100 K, occurring at 36.5 cm^{-1}, 49.67 cm^{-1}, and 74.62 cm^{-1}. Using the DFT-optimized structure, the vibrational frequencies and normal modes were calculated within the harmonic approximation, resulting in predicted IR-active modes at 37.31 cm^{-1}, 50.11 cm^{-1}, and

76.32 cm^{-1}. The motions involved in these transitions are complex and large-amplitude, and involve simultaneous external motions (i.e., translations) and internal motions (i.e., torsions). For example, the lowest energy transition involves the antisymmetric translation of adjacent rubrene molecules in the *b*-axis, coupled with a torsion of the phenyl groups with respect to the tetracene core (animations and figures of vibrational modes are available in the ESI).

The simulated frequencies are in excellent agreement with the experimental spectra, indicating that the utilized theoretical model is appropriately capturing the forces present in the solid. However, as with the structural optimization, the predicted frequencies are all over-estimated with respect to the experimental results, likely due to the more contracted 0 K structure exhibiting stiffer interatomic potentials compared to what is found at the experimental conditions.

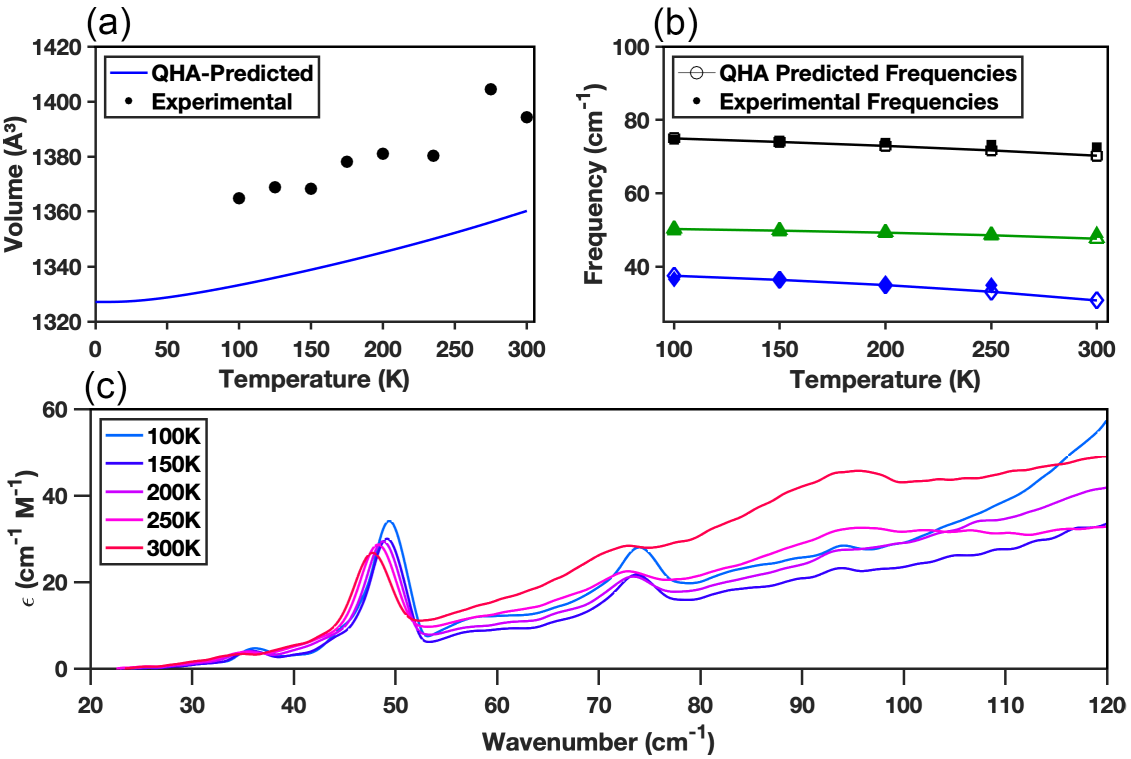

Figure 2: Temperature evolution of rubrene structure and dynamics. (a) QHA-predicted (blue line) and experimentally measured[59] (black circles) unit cell volumes of rubrene. (b) QHA-predicted (solid lines and open markers) and experimentally measured (filled markers) terahertz absorption frequencies of rubrene. (c) Experimental terahertz spectra.

Temperature Evolution

The properties of molecular crystals are strongly influenced by temperature, largely because of the weak non-covalent binding forces, but also because many of these interactions are anharmonic. While DFT simulations enable understanding observed phenomena, even the best comparisons are hindered by the zero-temperature limit of quantum mechanical methods. Traditionally, this necessitates experimental environments where the samples are cooled to the greatest extent possible, but in many cases such conditions are difficult to achieve.

In the case of rubrene, the structural evolution with temperature (100 K - 300 K) has previously been studied by Jurchescu et al.[59] using single-crystal X-ray diffraction experiments. As the temperature is increased, an expansion is observed along each unit cell axis, with the largest change occurring in the c-direction, which expands by 0.22 Å (or 1.56%) between the 100 K and 293 K experiments, while the a- and b-axes expand by +0.26% and +0.32%, respectively. Similarly, all of the observed spectral features in the THz-TDS spectra red-shift as a function of increasing temperature, indicating a softening of the intermolecular potentials, and thus weakening intermolecular forces. Additionally, due to increased thermally-activated relaxation pathways and decreased vibrational lifetimes, the spectral features simultaneously broaden with increasing temperature, a common trait of organic molecular crystals.

In order to predict these temperature-induced changes to the forces, structures, and dynamics, the quasi-harmonic approximation (QHA) method was utilized. The QHA method relies on the simulation of the structures and vibrational frequencies as a function of crystalline volume, which yields the volume-dependent structures, phonon modes, and associated thermodynamic parameters. Through the minimization of the volume- and temperature-dependent Helmholtz free energies, the volumes can be mapped to temperature values, yielding temperature-dependent structures, phonon modes, and related effects. It is important to note that this methodology does not contain any fixed parameters, as the various calculations are performed at a constrained volume while allowing each individual parameter (e.g. lattice vectors) to freely-relax within a volume constraint.

In the case of rubrene, four volumes were explored, corresponding to $-2\%, 0\%, +2\%$, and $+4\%$ volume increments, with respect to the fully-optimized solid. The QHA-predicted temperature evolution of the unit cell is shown in **Figure 2**. While there is a slight offset in the absolute magnitude of the predicted volumes (a difference of $\sim 30\,\text{Å}^3$ or $\sim 2\%$), the overall trend is well-captured by the theoretical model. Additionally, the temperature-dependent structures enable more accurate comparisons with experiment to be made. For example, the errors in the unit cell dimensions compared to the 100 K experimental values are significantly reduced when using the QHA-predicted 100 K structure, yielding errors in a, b, and c of -1.33%, -0.23%, and -0.76%, which ultimately reduces the errors compared to the 0 K optimization by approximately half.

Mirroring the successful modeling of the temperature-evolution of the structural parameters, the predicted evolution of the terahertz vibrational modes is also in excellent agreement with the experimental data. The theoretical predictions are in agreement with both the absolute values of the experimental transition frequencies, as well as the trends. An important note is that due to peak broadening, the lowest-frequency mode in rubrene is not reliably detectable at 300 K, making a direct comparison not possible for that particular mode at that particular temperature. Nonetheless, the successful reproduction of the structures and terahertz spectra of rubrene as a function of temperature indicates that the QHA simulation provides an accurate description of the interatomic forces over the range of explored temperatures, and enables more detailed analyses to be performed with confidence.

The agreement between simulated and experimental temperature evolution of the structure and dynamics of rubrene lends confidence that the forces present in the solid are well-modeled across the range of explored volumes (and by extension, temperatures). Additionally, as previously highlighted, low-frequency dynamics involve the forces most critical to the elastic properties of solids, since these modes often involve the same weak intermolecular interactions that are perturbed during mechanical processes.[28–30] Therefore, the successful modeling of the low-frequency dynamics as a function of temperature implies that the

associated elastic response would be equally well-modeled by the theory.

The elastic tensor is calculated using CRYSTAL through a fully-automated procedure.[55,56] Briefly, a previously fully relaxed structure is strained (with the number of applied strains determined by the crystal symmetry, up to a maximum of six), and subsequently the atomic positions are relaxed within the strained lattice configuration. Analytical energy gradients are then computed at each relaxed strained configuration. Each applied strain yields a set of components of the elastic tensor (from finite differences of the analytical gradients), which is then used to determine the mechanical properties of the solid.

Thermoelastic Response

Initially, the elastic response of rubrene was determined using the static (i.e., 0 K) structure, with the three-dimensional Young's modulus shown in **Figure 3**. The response is highly anisotropic, with lobes of high mechanical stiffness located along the *a*-axis, as well as two major components oriented orthogonally in the *bc*-plane. The origins of these particularly stiff directions can be described in terms of the bulk structure of rubrene, and is shown schematically in the ESI. The structure is dominated by interlocking molecules to maximize π-stacking. Thus, the major directions of mechanical stiffness involve those that result in an unfavorable interaction between adjacent molecules, where both the core and the substituents play a significant role.

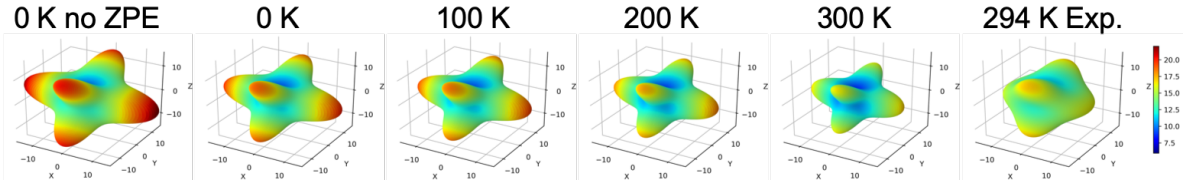

Figure 3: Predicted temperature evolution of the elastic response (Young's modulus) of rubrene in GPa, with the experimental data shown on the far-right.

The mechanical response of crystalline rubrene has been experimentally determined previously by Zhang et al.[60] at 294 K using Brillouin light scattering (BLS), and the three-dimensional Young's modulus is also shown in **Figure 3**. As can be readily observed,

the experimental data, while showing a similar qualitative anisotropic mechanical response, describe a much softer mechanical behavior than what is predicted from the 0 K static simulation from a quantitative point of view. A comparison of the directional Young modulus (i.e., the mechanical stiffness along each Cartesian direction) as shown in **Table 1**, highlights that the 0 K static simulation overestimates most values, particularly along the x (or a) axis. However, such an overestimation of the Young's moduli is expected from static calculations as thermal expansion effects are neglected and calculations are therefore performed on a significantly contracted structure.

In order to take into account the temperature evolution of the forces and associated three-dimensional structures, the QHA-determined structural evolution was used as the basis for calculating the elastic response as a function of temperature. The QHA-determined thermal expansion was used to perform constrained volume optimizations corresponding to the 100 K, 200 K, and 300 K volumes. Additionally, we have also performed a physically-relevant 0 K optimization, through the inclusion of zero-point energy. Subsequently, the optimized structures were then used to simulate the elastic response, with the results presented in **Figure 3**.

The temperature evolution of the mechanical response of rubrene is characterized by a systematic softening in all directions as temperature is increased. This mirrors the thermal expansion effects of the structures and terahertz dynamics, where all axes expand and all modes red-shift with increasing temperature, indicating a softening of the intermolecular forces. A more quantitative comparison can be made through the evaluation of the directional Young moduli, which soften by 31.1%, 27.7%, and 35.6% between the static 0 K and 300 K

Table 1: Predicted and experimental[60] directional Young moduli (GPa) of rubrene, and the differences with respect to experiment for the 300 K data (Δ).

	$0\,K_{PBE}$	$300\,K_{PBE}$	$300\,K_{PBE0}$	Exp.	Δ_{PBE}	Δ_{PBE0}
E_x	22.05	15.19	14.88	14.10	1.09	0.77
E_y	9.72	7.02	8.31	9.01	-1.99	-0.70
E_z	5.96	3.83	4.88	7.70	-3.87	-2.83

simulations, respectively (**Figure 1**). Again, as mirrored in the structural evolution, the c-axis undergoes a larger thermal expansion than the other two axes, which is captured in the elastic information.

Comparing the 300 K prediction with the experimental results, the simulated elastic tensor is in much better agreement compared to the 0 K simulation. The directional Young moduli highlight the successful modeling of the elastic response, with only the E_z value (the smallest one) deviating from the experimental result. It is important to note that this 300 K predicted elastic response does not contain any fixed structural parameters, and is purely first-principles result. This highlights the utility of this methodology, as previous studies must rely on constraining the structures significantly to their high-temperature form, necessitating the knowledge of the structure and temperature evolution of the structure in order to produce comparable results.

While the elastic response using the PBE functional is in good general agreement with the experimental results, it is well-known that hybrid functionals often yield a more accurate representation of interatomic forces.[61] However, hybrid functionals simultaneously come with a significantly increased computational cost, making the QHA calculation and subsequent elastic analyses incredibly cost-prohibitive. In order to circumvent this, while achieving the improved accuracy of a hybrid functional, a proposed solution involves using the PBE-predicted thermal expansion and applying the appropriate thermal expansion to a fully-optimized structure using a hybrid functional, followed by the elastic analysis using a hybrid functional. We have utilized this methodology here, by using the PBE0 functional to fully optimize the structure without any constraints, followed by scaling the volume by the PBE-QHA-determined thermal expansion coefficient, and then performing a constrained volume optimization and elastic analysis with PBE0. The resulting elastic tensor, while generally similar to the PBE case, offers a modest improvement and better overall agreement with the experimental results. This is illustrated in **Table 1**, where each component of the directional Young moduli is in better agreement with the experimental results compared to the PBE

case.

BTBT

While experimental elastic tensor information exists for crystalline rubrene, it is far from trivial to obtain such data on materials (particularly so for low-symmetry crystals), often requiring complicated experimental setups or time at national laboratories (in the case of BLS experiments, a neutron source), in addition to requiring large single crystals. Thus, we propose that based on the previous results, an adequate representation of the structures and forces, determined through far more manageable experiments within the academic laboratory, coupled with the QHA thermoelastic calculations, provides an alternate route to the full determination of the thermoelastic response of materials.

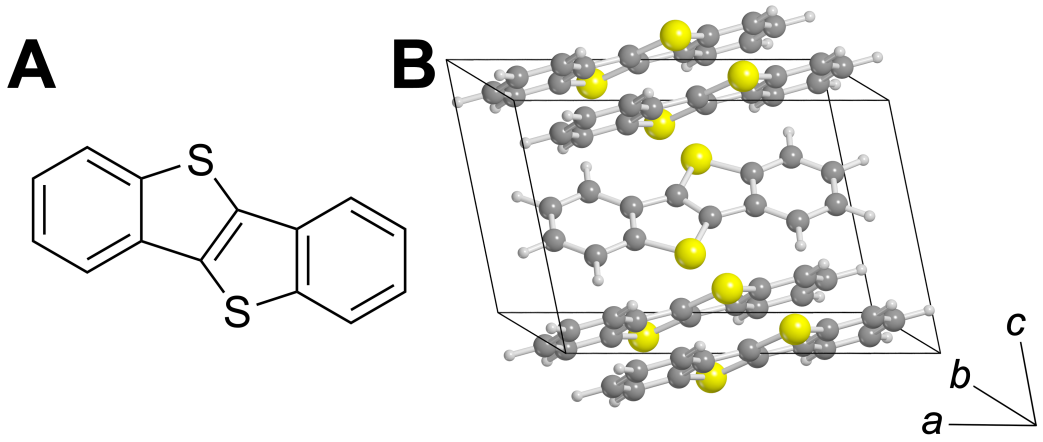

Figure 4: Molecular structure (**A**) and unit cell structure (**B**) of organic semiconductor BTBT.

Structural Analysis

To highlight this, we have investigated the popular OSC, [1]benzothieno[3,2-b][1]benzothiophene (BTBT). BTBT crystallizes in the monoclinic $P21/c$ space group (**Figure 4**) with 2 molecules in the unit cell, and lattice parameters of $a = 11.82\,\text{Å}$, $b = 5.88\,\text{Å}$, $c = 7.98\,\text{Å}$, and $\beta = 106.12°$ at 100 K. Similar to rubrene, the molecules in the lattice are oriented in a

herringbone packing motif to maximize π-stacking, with π-stacking primarily along the c-unit cell axis.

We have performed single-crystal XRD diffraction measurements to determine the structure of BTBT at three temperatures, 100 K, 200 K, and 300 K. The temperature evolution involves a slight expansion of the a- and b-unit cell axes between 100 K and 300 K (+0.86% and +0.68%, respectively), with the largest change occurring in the c-axis (+2.37%) – attributed to the soft intermolecular interactions along that coordinate.

The crystal structure of BTBT contains significantly fewer atoms compared to rubrene, and permits the use of a larger basis set. Therefore, the triple-zeta 6-311G(2d,2p) basis set was used, along with the PBE functional and coupled with the D3 dispersion correction. The simulated QHA results are in excellent agreement with the experimental thermal expansion, with the theory overestimating the unit cell volume by $< 5\,\text{Å}^3$ across the range of explored temperatures (an error of $< 1\%$), as shown in **Figure 5**. Importantly, the trend in the thermal expansion is captured to a high-degree of accuracy, highlighting the robust numerical accuracy of the simulation.

Low-Frequency Dynamics

The variable-temperature terahertz spectrum of BTBT displays four prominent spectral features between $0 - 120\,\text{cm}^{-1}$ (**Figure 5**), occurring at 57.86, 66.85, 89.33, and $104.41\,\text{cm}^{-1}$. The results of the 100 K QHA-simulation is in excellent agreement with experiment, predicting features at 59.95, 68.00, 90.49, and $101.39\,\text{cm}^{-1}$, respectively. Like rubrene, the motions associated with these modes involve external, internal, and mixed mode-types, for example the lowest frequency mode which is primarily an external translation along the b-axis (animations available in the ESI).

The temperature-dependence of the vibrational frequencies is equally well-predicted by the QHA analysis (**Figure 5**). Like rubrene, all modes exhibit a red-shift with increasing temperature, indicating a softening of the intermolecular potential. For the three lowest-

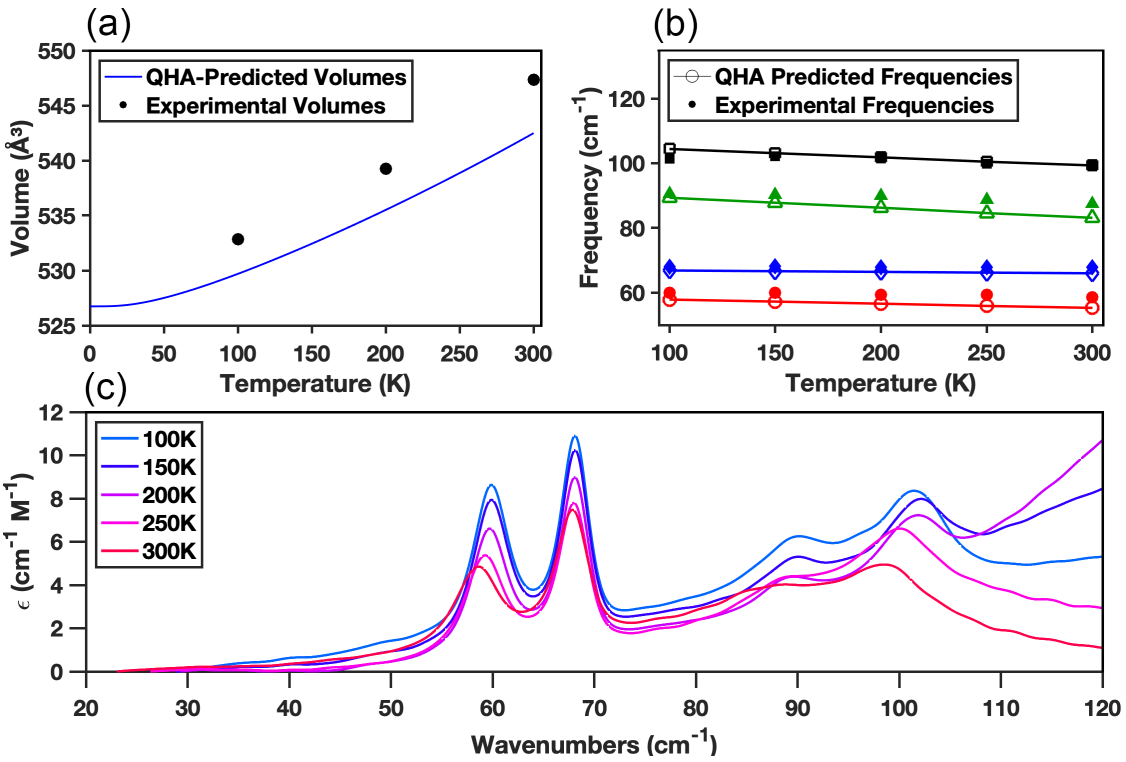

Figure 5: Temperature evolution of the BTBT structure and dynamics. (a) QHA-predicted (blue line) and experimentally measured (black circles) unit cell volumes of BTBT. (b) QHA-predicted (solid lines and open markers) and experimentally measured (filled markers) terahertz absorption frequencies of BTBT. (c) Experimental terahertz spectra.

frequency modes, the predicted transitions are slightly underestimated with respect to the experimental frequencies. However, these discrepancies are $< 5\,\mathrm{cm}^{-1}$.

Thermoelastic Response

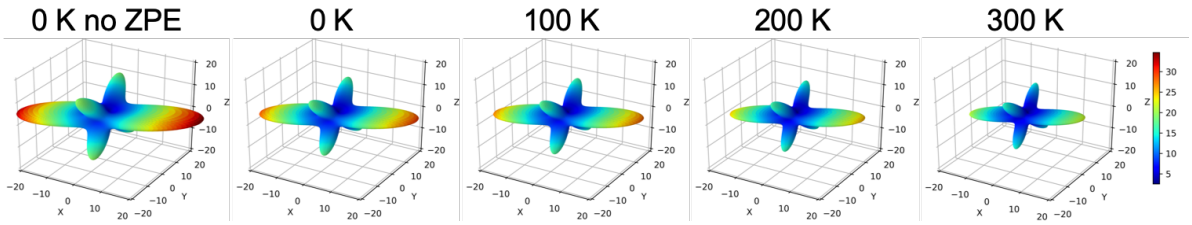

Figure 6: Predicted temperature evolution of the elastic response (Young's modulus) of BTBT in GPa.

The different bulk packing arrangement of BTBT compared to rubrene suggests that the forces, and by extension, the mechanical properties, will be significantly different between the two solids. Indeed, the mechanical response of BTBT at 0 K is significantly anisotropic, with the major π-stacking directions yielding a relatively soft mechanical response, while the non-stacking direction is mechanically stiffer. The origins of this mechanical stiffness along the a-axis arise from the proximity of neighboring molecules. The interlocking herringbone nature of the solid locks the molecules into their positions, with relatively close contact along the a-axis due to the lack of any significant non-covalent interactions in this dimension. However, compression along this axis simultaneously results in two destabilizing interactions, the repulsion from adjacent molecules due to spatial proximity, as well as the loss of stabilizing intermolecular π-stacking interactions upon compression, which ultimately explain the large mechanical stiffness. This has implications for charge transport, as previously it has been shown that longitudinal translations of the BTBT molecules result in significant fluctuations in the charge transport integral due to disruptions in the π-stacking interaction, which drastically increases dynamic disorder and hinders mobility.[62]

The temperature-evolution of the mechanical response of BTBT is characterized by a systematic softening of all components. In particular, the a-axis undergoes the most drastic

Table 2: Predicted directional Young moduli (GPa) of BTBT as a function of temperature.

	0K no ZPE	0K	100K	200K	300K
E_x	30.46	25.91	24.44	21.99	18.59
E_y	6.03	5.15	4.83	4.35	3.76
E_z	4.61	3.93	3.70	3.38	2.95

change. This is readily apparent when considering the directional Young moduli, as shown in **Table 2**. This is likely due to the expansion along the a-axis reducing the steric hinderance upon compression strain, ultimately softening that direction dramatically. However, in relative terms, all of the components soften by nearly the same amounts, corresponding to a 39%, 38%, and 36% reduction in stiffness between 0 K and 300 K for E_x, E_y, and E_z, respectively.

Conclusions

Overall, the thermoelastic response was fully determined for two well-studied organic semiconducting crystals, rubrene and BTBT, using solid-state density functional theory simulations and terahertz time-domain spectroscopy measurements. The temperature evolution of the structures, dynamics, and forces was predicted using quasi-harmonic approximation simulations, and the results validated against experimental single-crystal X-ray diffraction and terahertz spectroscopic results. The effective prediction of the low-frequency vibrational spectra and thermal expansion effects indicates that the theoretical model sufficiently reproduced the intermolecular forces with a high-degree of accuracy, and therefore enabled the confident determination of the elastic tensor as a function of temperature. The results highlight the robustness of this methodology and provide a framework for further study into this important area of materials chemistry.

Conflicts of interest

There are no conflicts to declare.

Acknowledgements

P.A.B, M.A.M, and M.T.R thank the University of Vermont for its continued support. M.A.M thanks the University of Vermont A. Paul Krapcho Chemistry Summer Fellowship for support.

References

(1) Sirringhaus, H. 25th Anniversary Article: Organic Field-Effect Transistors: The Path Beyond Amorphous Silicon. *Adv. Mater.* **2014**, *26*, 1319–1335.

(2) Itskos, G.; Othonos, A.; Rauch, T.; Tedde, S. F.; Hayden, O.; Kovalenko, M. V.; Heiss, W.; Choulis, S. A. Optical Properties of Organic Semiconductor Blends with Near-Infrared Quantum-Dot Sensitizers for Light Harvesting Applications. *Adv. Energy Mater.* **2011**, *1*, 802–812.

(3) Root, S. E.; Savagatrup, S.; Printz, A. D.; Rodriquez, D.; Lipomi, D. J. Mechanical Properties of Organic Semiconductors for Stretchable, Highly Flexible, and Mechanically Robust Electronics. *Chem. Rev.* **2017**, *117*, 6467–6499.

(4) Lee, S. H.; Park, H.; Kim, S.; Son, W.; Cheong, I. W.; Kim, J. H. Transparent and flexible organic semiconductor nanofilms with enhanced thermoelectric efficiency. *J. Mater. Chem. A* **2014**, *2*, 7288–7294.

(5) Gupta, S. K.; Jha, P.; Singh, A.; Chehimi, M. M.; Aswal, D. K. Flexible organic semiconductor thin films. *J. Mater. Chem. C* **2015**, *3*, 8468–8479.

(6) Kim, S.-J.; Song, J.-M.; Lee, J.-S. Transparent organic thin-film transistors and non-volatile memory devices fabricated on flexible plastic substrates. *J. Mater. Chem.* **2011**, *21*, 14516.

(7) Qian, Y.; Zhang, X.; Xie, L.; Qi, D.; Chandran, B. K.; Chen, X.; Huang, W. Stretchable Organic Semiconductor Devices. *Adv. Mater.* **2016**, *28*, 9243–9265.

(8) Kim, C.; Facchetti, A.; Marks, T. J. Probing the Surface Glass Transition Temperature of Polymer Films via Organic Semiconductor Growth Mode, Microstructure, and Thin-Film Transistor Response. *J. Am. Chem. Soc.* **2009**, *131*, 9122–9132.

(9) Wang, Z.; Zhang, J.; Xing, R.; Yuan, J.; Yan, D.; Han, Y. Micropatterning of Organic Semiconductor Microcrystalline Materials and OFET Fabrication by "Hot Lift Off". *J. Am. Chem. Soc.* **2003**, *125*, 15278–15279.

(10) Savagatrup, S.; Printz, A. D.; O'Connor, T. F.; Zaretski, A. V.; Rodriquez, D.; Sawyer, E. J.; Rajan, K. M.; Acosta, R. I.; Root, S. E.; Lipomi, D. J. Mechanical degradation and stability of organic solar cells: molecular and microstructural determinants. *Energy & Environmental Science* **2015**, *8*, 55–80.

(11) Brillante, A.; Bilotti, I.; Della Valle, R. G.; Venuti, E.; Girlando, A. Probing polymorphs of organic semiconductors by lattice phonon Raman microscopy. *CrystEngComm* **2008**, *10*, 937.

(12) Jurchescu, O. D.; Mourey, D. A.; Subramanian, S.; Parkin, S. R.; Vogel, B. M.; Anthony, J. E.; Jackson, T. N.; Gundlach, D. J. Effects of polymorphism on charge transport in organic semiconductors. *Phys. Rev. B* **2009**, *80*.

(13) Daniel Głowacki, E.; Leonat, L.; Irimia-Vladu, M.; Schwödiauer, R.; Ullah, M.; Sitter, H.; Bauer, S.; Serdar Sariciftci, N. Intermolecular hydrogen-bonded organic semiconductors—Quinacridone versus pentacene. *Appl. Phys. Lett.* **2012**, *101*, 023305.

(14) Li, M.; Balawi, A. H.; Leenaers, P. J.; Ning, L.; Heintges, G. H. L.; Marszalek, T.; Pisula, W.; Wienk, M. M.; Meskers, S. C. J.; Yi, Y. et al. Impact of polymorphism on the optoelectronic properties of a low-bandgap semiconducting polymer. *Nat. Commun.* **2019**, *10*.

(15) Martinelli, N. G.; Olivier, Y.; Athanasopoulos, S.; Delgado, M.-C. R.; Pigg, K. R.; da Silva Filho, D. A.; Sánchez-Carrera, R. S.; Venuti, E.; Valle, R. G. D.; Brédas, J.-L. et al. Influence of Intermolecular Vibrations on the Electronic Coupling in Organic Semiconductors: The Case of Anthracene and Perfluoropentacene. *ChemPhysChem* **2009**, *10*, 2265–2273.

(16) Della Valle, R. G.; Fracassi, P. F.; Righini, R.; Califano, S. Anharmonic processes in molecular crystals. Calculation of the anharmonic shifts, bandwidths and energy decay processes in crystalline naphthalene. *Chem. Phys.* **1983**, *74*, 179–195.

(17) King, M. D.; Buchanan, W. D.; Korter, T. M. Investigating the Anharmonicity of Lattice Vibrations in Water-Containing Molecular Crystals through the Terahertz Spectroscopy ofl-Serine Monohydrate. *J. Phys. Chem. A* **2010**, *114*, 9570–9578.

(18) Barron, T. H. K.; Collins, J. G.; White, G. K. Thermal expansion of solids at low temperatures. *Adv. Phys.* **1980**, *29*, 609–730.

(19) Varughese, S.; Kiran, M. S. R. N.; Ramamurty, U.; Desiraju, G. R. Nanoindentation in Crystal Engineering: Quantifying Mechanical Properties of Molecular Crystals. *Angew. Chem. Int. Ed.* **2013**, *52*, 2701–2712.

(20) Mante, F. K.; Baran, G. R.; Lucas, B. Nanoindentation studies of titanium single crystals. *Biomaterials* **1999**, *20*, 1051–1055.

(21) Nowak, R.; Pessa, M.; Suganuma, M.; Leszczynski, M.; Grzegory, I.; Porowski, S.; Yoshida, F. Elastic and plastic properties of GaN determined by nano-indentation of bulk crystal. *Appl. Phys. Lett.* **1999**, *75*, 2070–2072.

(22) Casari, C. S.; Bassi, A. L.; Bottani, C. E.; Barborini, E.; Piseri, P.; Podestà, A.; Milani, P. Acoustic phonon propagation and elastic properties of cluster-assembled carbon films investigated by Brillouin light scattering. *Phys. Rev. B* **2001**, *64*, 085417.

(23) Faurie, D.; Djemia, P.; Le Bourhis, E.; Renault, P.-O.; Roussigné, Y.; Chérif, S. M.; Brenner, R.; Castelnau, O.; Patriarche, G.; Goudeau, P. Elastic anisotropy of polycrystalline Au films: Modeling and respective contributions of X-ray diffraction, nanoindentation and Brillouin light scattering. *Acta Mater.* **2010**, *58*, 4998–5008.

(24) Djemia, P.; Roussigné, Y.; Dirras, G. F.; Jackson, K. M. Elastic properties of β-SiC films by Brillouin light scattering. *J. Appl. Phys.* **2004**, *95*, 2324–2330.

(25) Schmuttenmaer, C. A. Exploring Dynamics in the Far-Infrared with Terahertz Spectroscopy. *Chem. Rev.* **2004**, *104*, 1759–1780.

(26) Ruggiero, M. T. Invited Review: Modern Methods for Accurately Simulating the Terahertz Spectra of Solids. *Journal of Infrared, Millimeter, and Terahertz Waves* **2020**,

(27) Zhang, W.; Maul, J.; Vulpe, D.; Moghadam, P. Z.; Fairen-Jimenez, D.; Mittleman, D. M.; Zeitler, J. A.; Erba, A.; Ruggiero, M. T. Probing the Mechanochemistry of Metal–Organic Frameworks with Low-Frequency Vibrational Spectroscopy. *J. Phys. Chem. C* **2018**, *122*, 27442–27450.

(28) Ruggiero, M. T.; Sibik, J.; Orlando, R.; Zeitler, J. A.; Korter, T. M. Measuring the Elasticity of Poly-l -Proline Helices with Terahertz Spectroscopy. *Angew. Chem. Int. Ed.* **2016**, *55*, 6877–6881.

(29) Maul, J.; Ryder, M. R.; Ruggiero, M. T.; Erba, A. Pressure-driven mechanical anisotropy and destabilization in zeolitic imidazolate frameworks. *Phys. Rev. B* **2019**, *99*.

(30) Ryder, M. R.; Civalleri, B.; Cinque, G.; Tan, J.-C. Discovering connections between terahertz vibrations and elasticity underpinning the collective dynamics of the HkuSt-1 metal–organic framework. *CrystEngComm* **2016**, *18*, 4303–4312.

(31) Ruggiero, M. T.; Zeitler, J. A.; Erba, A. Intermolecular anharmonicity in molecular crystals: interplay between experimental low-frequency dynamics and quantum quasi-harmonic simulations of solid purine. *Chem. Commun.* **2017**, *53*, 3781–3784.

(32) Dampf, S. J.; Korter, T. M. Anomalous Temperature Dependence of the Lowest-Frequency Lattice Vibration in Crystalline γ-Aminobutyric Acid. *J. Phys. Chem. A* **2019**, *123*, 2058–2064.

(33) Day, G. M.; Zeitler, J. A.; Jones, W.; Rades, T.; Taday, P. F. Understanding the Influence of Polymorphism on Phonon Spectra: Lattice Dynamics Calculations and Terahertz Spectroscopy of Carbamazepine. *J. Phys. Chem. B* **2006**, *110*, 447–456.

(34) Ruggiero, M. T.; Zeitler, J. A. Resolving the Origins of Crystalline Anharmonicity Using Terahertz Time-Domain Spectroscopy and ab Initio Simulations. *J. Phys. Chem. B* **2016**, *120*, 11733–11739.

(35) Fan, S.; Ruggiero, M. T.; Song, Z.; Qian, Z.; Wallace, V. P. Correlation between saturated fatty acid chain-length and intermolecular forces determined with terahertz spectroscopy. *Chem. Commun.* **2019**, *55*, 3670–3673.

(36) Erba, A.; Maul, J.; Civalleri, B. Thermal properties of molecular crystals through dispersion-corrected quasi-harmonic ab initio calculations: the case of urea. *Chem. Commun.* **2016**, *52*, 1820–1823.

(37) Brandenburg, J. G.; Potticary, J.; Sparkes, H. A.; Price, S. L.; Hall, S. R. Thermal expansion of carbamazepine: systematic crystallographic measurements challenge quantum chemical calculations. *J. Phys. Chem. Lett.* **2017**, *8*, 4319–4324.

(38) McKinley, J. L.; Beran, G. J. O. Improving predicted nuclear magnetic resonance chemical shifts using the quasi-harmonic approximation. *J. Chem. Theory Comput.* **2019**, *15*, 5259–5274.

(39) Erba, A. On combining temperature and pressure effects on structural properties of crystals with standardab initiotechniques. *J. Chem. Phys.* **2014**, *141*, 124115.

(40) Erba, A.; Shahrokhi, M.; Moradian, R.; Dovesi, R. On how differently the quasi-harmonic approximation works for two isostructural crystals: Thermal properties of periclase and lime. *J. Chem. Phys.* **2015**, *142*, 044114.

(41) Saito, M.; Osaka, I.; Miyazaki, E.; Takimiya, K.; Kuwabara, H.; Ikeda, M. One-step synthesis of [1]benzothieno[3,2-b][1]benzothiophene from o-chlorobenzaldehyde. *Tetrahedron Lett.* **2011**, *52*, 285–288.

(42) Sheldrick, G. M. *SADABS, program for empirical absorption correction of area detector data*; University of Göttingen, 1996.

(43) Dovesi, R.; Erba, A.; Orlando, R.; Zicovich-Wilson, C. M.; Civalleri, B.; Maschio, L.; Rérat, M.; Casassa, S.; Baima, J.; Salustro, S. et al. Quantum-mechanical condensed matter simulations with CRYSTAL. *WIREs Comput. Mol. Sci.* **2018**, *8*, e1360.

(44) Perdew, J. P.; Burke, K.; Ernzerhof, M. Generalized Gradient Approximation Made Simple. *Phys. Rev. Lett.* **1996**, *77*, 3865–3868.

(45) Adamo, C.; Barone, V. Toward reliable density functional methods without adjustable parameters: The PBE0 model. *J. Chem. Phys.* **1999**, *110*, 6158–6170.

(46) Grimme, S.; Antony, J.; Ehrlich, S.; Krieg, H. A consistent and accurate ab initio parametrization of density functional dispersion correction (Dft-D) for the 94 elements H-pu. *J. Chem. Phys.* **2010**, *132*, 154104.

(47) Grimme, S.; Ehrlich, S.; Goerigk, L. Effect of the damping function in dispersion corrected density functional theory. *J. Comput. Chem.* **2011**, *32*, 1456–1465.

(48) Hehre, W. J.; Ditchfield, R.; Pople, J. A. Self—Consistent Molecular Orbital Methods. XII. Further Extensions of Gaussian—Type Basis Sets for Use in Molecular Orbital Studies of Organic Molecules. *J. Chem. Phys.* **1972**, *56*, 2257–2261.

(49) Hariharan, P. C.; Pople, J. A. The influence of polarization functions on molecular orbital hydrogenation energies. *Theor. Chim. Acta* **1973**, *28*, 213–222.

(50) Krishnan, R.; Binkley, J. S.; Seeger, R.; Pople, J. A. Self-consistent molecular orbital methods. XX. A basis set for correlated wave functions. *J. Chem. Phys.* **1980**, *72*, 650–654.

(51) Pascale, F.; Zicovich-Wilson, C. M.; López Gejo, F.; Civalleri, B.; Orlando, R.; Dovesi, R. The calculation of the vibrational frequencies of crystalline compounds and its implementation in the CryStaL code. *J. Comput. Chem.* **2004**, *25*, 888–897.

(52) Zicovich-Wilson, C. M.; Pascale, F.; Roetti, C.; Saunders, V. R.; Orlando, R.; Dovesi, R. Calculation of the vibration frequencies of α-quartz: The effect of Hamiltonian and basis set. *J. Comput. Chem.* **2004**, *25*, 1873–1881.

(53) Erba, A.; Maul, J.; Civalleri, B. Thermal properties of molecular crystals through dispersion-corrected quasi-harmonic ab initio calculations: the case of urea. *Chem. Commun.* **2016**, *52*, 1820–1823.

(54) Erba, A.; Maul, J.; Demichelis, R.; Dovesi, R. Assessing thermochemical properties of materials through ab initio quantum-mechanical methods: the case of α-Al_2O_3. *Phys. Chem. Chem. Phys.* **2015**, *17*, 11670–11677.

(55) Perger, W. F.; Criswell, J.; Civalleri, B.; Dovesi, R. Ab-initio calculation of elastic

constants of crystalline systems with the CRYSTAL code. *Comput. Phys. Commun.* **2009**, *180*, 1753–1759.

(56) Erba, A.; Mahmoud, A.; Orlando, R.; Dovesi, R. Elastic properties of six silicate garnet end members from accurate ab initio simulations. *Phys. Chem. Miner.* **2013**, *41*, 151–160.

(57) Destefanis, M.; Ravoux, C.; Cossard, A.; Erba, A. Thermo-elasticity of materials from quasi-harmonic calculations. *Minerals* **2019**, *9*, 16.

(58) Takeya, J.; Yamagishi, M.; Tominari, Y.; Hirahara, R.; Nakazawa, Y.; Nishikawa, T.; Kawase, T.; Shimoda, T.; Ogawa, S. Very high-mobility organic single-crystal transistors with in-crystal conduction channels. *Appl. Phys. Lett.* **2007**, *90*, 102120.

(59) Jurchescu, O. D.; Meetsma, A.; Palstra, T. T. Low-temperature structure of rubrene single crystals grown by vapor transport. *Acta Crystallogr. B* **2006**, *9*, 330–334.

(60) Zhang, Y.; Manke, D. R.; Sharifzadeh, S.; Briseno, A. L.; Ramasubramaniam, A.; Koski, K. J. The elastic constants of rubrene determined by Brillouin scattering and density functional theory. *Appl. Phys. Lett.* **2017**, *110*, 071903.

(61) Ruggiero, M. T.; Gooch, J.; Zubieta, J.; Korter, T. M. Evaluation of range-corrected density functionals for the simulation of pyridinium-containing molecular crystals. *J. Phys. Chem. A* **2016**, *120*, 939–947.

(62) Schweicher, G.; D'Avino, G.; Ruggiero, M. T.; Harkin, D. J.; Broch, K.; Venkateshvaran, D.; Liu, G.; Richard, A.; Ruzié, C.; Armstrong, J. et al. Chasing the "Killer" Phonon Mode for the Rational Design of Low-Disorder, High-Mobility Molecular Semiconductors. *Adv. Mater.* **2019**, *31*, 1902407.